May – June 2020
ISSN: 0193-4120 Page No. 2659 - 2673

Laser Heat Treatment was Performed to Improve the Bending Property of Laser Welded Joints o Low-Alloy Ultrahigh-Strength Steel with Minimized Strength Loss

[1]S Sampath Kumar, [2]K V Sai Pavan, [3]T.Rajasanthosh Kumar, [4]Manikyam Sandeep
[1,2,3]Department of mechanical engineering, Matrusri engineering college
[4]Ace engineering college
Hyderabad, telangana state

Article Info
Volume 83
Page Number: 2659 - 2673
Publication Issue:
May - June 2020

Abstract:

The poor twisting property of laser-welded joints constrains the utilization of low-amalgam ultrahigh-quality steel (LAUHSS). Right now, phases of laser heat treatment (LHT) were performed to improve the face-and back-twisting property of joints with limited quality misfortune. The microstructures and mechanical properties were assessed, and the impact system of LHT on the bowing property was talked about. The first LHT meant to improve the back-bowing property, after which the joints were contained the austenized and treating zones. In the treating zone, the first inhomogeneous microstructures changed into comparative tempered martensite. This smoothed out the precarious hardness slope to generally uniform qualities. In the austenized zone, austenization happened and the hardness valley despite everything existed around the sides of the zone. The mechanical property test results demonstrated the back-bowing edge could be improved from 30 deg to more than 90 deg, while the face-twisting point indicated inadmissible outcomes with more than 1280 MPa elasticity. The second LHT was performed dependent on the first LHT to improve the face-twisting property of joints. With lower power in the second LHT, the double stage microstructures in the austenized zone tempered. Also, the hardness circulations of joints would in general be progressively uniform without valleys. A more than 90-deg face-twisting point and around 1205 MPa elasticity were acquired. After LHT, the scope of plastic misshapening during the bowing procedure extended as opposed to packing in the hardness valley zone, which prompted a bigger relative twisting range and less tractable weight on the bowing surface. This is gainful for the improvement of the bowing property.

Article History
Article Received*: 11August 2019*
Revised*: 18November 2019*
Accepted*: 23January 2020*
Publication*: 10May2020*

KEYWORDS: *Low-Alloy Ultrahigh-Strength Steel - Bending Property -Laser-Welded Joints - Relative Bending Radius -Laser Heat Treatment*

I. INTRODUCTION

Eco-friendliness, security, and ecological effect are key issues for the car business, which is the main thrust for the utilization of low-amalgam ultrahigh-quality steel (LAUHSS) as a result of its useful blend of high quality/weight proportion and great strength (Refs. 1, 2). All in all, LAUHSS is utilized in the extinguished and tempered conditions (Refs. 1, 3).

Hardening at low temperature is done to get a high rigidity up to 1700 MPa, just as high hardness with the microstructures of martensite. The most fundamental welding strategy of LAUHSS is circular segment welding with filler metal (Refs. 4, 5).

May – June 2020
ISSN: 0193-4120 Page No. 2659 - 2673

In any case, related research has uncovered that rigidity of bend welded joints is commonly under 1000 MPa, and the joint proficiency (elasticity proportion of joints to base metal) is normally lower than 60% (Refs. 6–8) in light of the fact that the microstructures of weld metal (WM) for the most part comprise of the delicate stage, for example, austenite and □-ferrite (Refs. 8, 9).

Laser welding has become a productive method to improve joint quality, which gives a generally thin weld and limited warmth influenced zone (HAZ) because of its attributes of high force thickness and low warmth inputs (Refs. 10, 11). All the more critically, the fine martensite structure can be gotten in the weld, which adds to the comparative rigidity of joints in examination with the base metal (Ref. 12).

A few examinations on laser welding of LAUHSS with more than 1500 MPa rigidity show that up to 90% joint proficiency could be acquired (Refs. 12–14). Be that as it may, one of the most essential difficulties in the laser welding of LAUHSS is the poor formability of joints, particularly in the bowing property. It was accounted for (Ref. 15) that fiberlaser-welded joints of 0.3C–1Cr–1Si steel could simply curve to not exactly a 40-deg point before falling flat. For the bowing trial of laser-welded Armox 500T steel (Ref. 5), all the joints could simply arrive at 45–50 deg. The vast majority of the laser-welded joints of LAUHSS broke in the HAZ with little bowing points (Refs. 5, 15). Be that as it may, a twisting edge of 90 deg after springback is required in viable applications (Ref. 16).

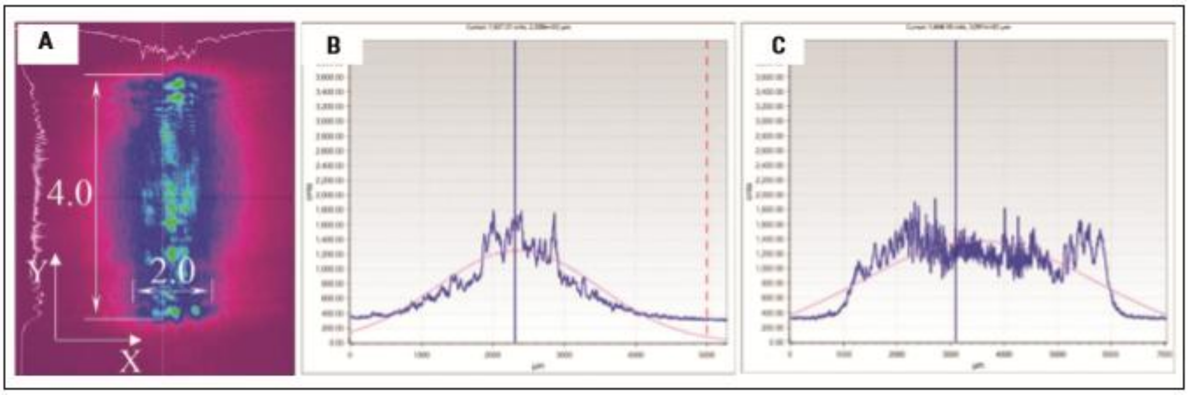

Fig. 1 — Light distribution of the rectangular spot: A — Overall energy distribution; B — energy distribution along the x-axis; C — energy distribution along the y-axis.

II. Material and Methods

Three 3-mm-thick, 1700-MPa LAUHSS plates with the elements of 60 □ 100 mm were utilized right now. The substance arrangements are recorded in Table 1. The as-provided condition of the steel was arrangement toughened in a latent situation at 800°C for 1 h, at that point oil cooled to room temperature, lastly tempered at 200°C for 1 h. Laser welding was acknowledged with an IPG YLS-2000 fiber laser. As an engaged spot is advantageous for misusing the benefits of laser welding, 0 mm was utilized in the welding progress. In light of the enhanced tests, the parameters of laser power, welding speed, and defocusing sum were 2.0 kW, 1.5 m/min, and 0 mm, individually. High-immaculateness argon was provided as the protecting gas with a stream pace of 15 L/min at the front and posteriors.

The equivalent IPG YLS-2000 fiber laser with an indispensable mirror was utilized for LHT. The standard of the incorporating mirror is that, as indicated by the geometrical optics, the conventional surface of transformation of the central mirror is supplanted by a multistrip bended surface of coordinating mirror (Ref. 38). Along these lines, in the wake of centering of the incorporating mirror, the laser bar would introduce the rectangular cut of

May – June 2020
ISSN: 0193-4120 Page No. 2659 - 2673

light with uniform appropriation of light power. The measurements and light conveyance of the spot are given in Fig. 1. A rectangular spot was created with measurements of about 4.0 × 1.0 mm, and the vitality was consistently dispersed. The schematic graph of the LHT is appeared in Fig. 2. As Fig. 2A shows, the laser responded along the weld in the scope of 20 mm width to do neighborhood warming on the top surface of tests. Bigger plates could be treated by filtering the surface with a cover.

As Fig. 2B appears, spacers were included between the examples and subplate to stifle heat dissemination. To improve both the face-and the back-twisting execution by single-face filtering, two phases of LHT (the first LHT and the second LHT) were performed. The first LHT was utilized to improve the back-twisting property, while the second LHT was utilized to improve the facebending property of joints after the first LHT. Before LHT, dark ink was applied as permeable on the top surface of tests to build the laser retention rate.

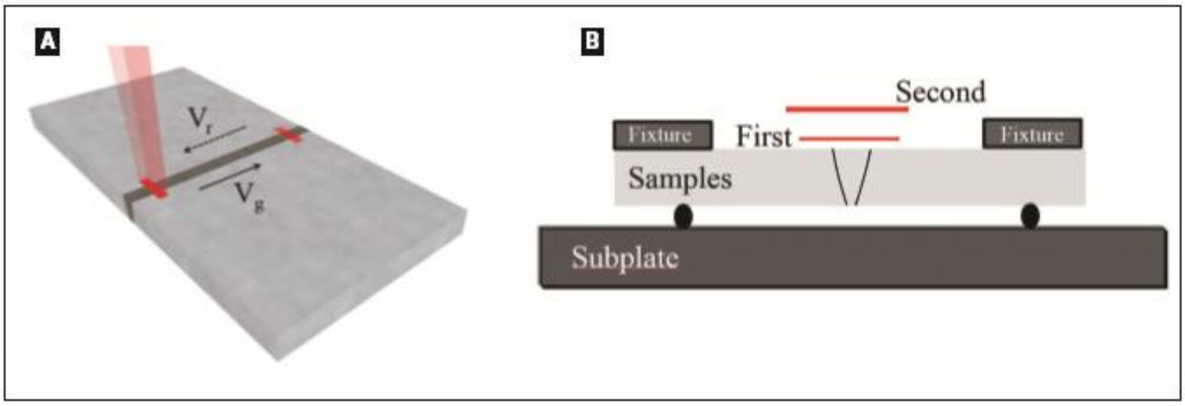

Fig. 2 — Schematic diagram of the LHT process: A — Scan path; B — installation diagram

The compelling constituent of dark ink utilized in the investigation was carbon dark. In the LHT procedure, the warmth move could be constrained by various parameters, yet no temperature estimation was utilized for this examination. The parameters of the two phases of the LHT procedure are given in Tables 2 and 3, individually. It could be discovered that multipath laser filtering systems were applied to get a sufficiently high temperature. The F-0 examples in Table 2 allude to the laser-welded joints without LHT. The microstructures of joints were seen with optical microscopy (OM) and examining electron microscopy (SEM) joined with vitality dispersive spectrometer (EDS). Before microstructure perception, the examples were cut, cleaned, and scratched with changed Fry's reagent (50 mL HCL + 25 mL HNO3 + 1 g CuCl2 + 150 mL H2O). Hardness estimations were performed on cross areas of joints utilizing a Vickers hardness analyzer at 500 g/15 s. The test position was situated at 0.15 mm from the face and back. Bowing and malleable tests were performed. The extents of test tests and the exploratory gadget of twist are given in Fig. 3. It very well may be discovered that multiple times the punch breadth was utilized for the twisting test. The twisting test was performed by the ISO 5173:2000 standard. The greatest bowing edge was controlled at 90 deg. The weld fortification on the face and back areas was expelled by manual crushing before the mechanical property tests.

Table 1 — Main Chemical Components of Base Metal (wt-%)

C	Mn	Cr	Mo	Ni	Si	Nb	Fe
0.3	0.3	0.8	0.3	0.8	0.3	0.05	other

May – June 2020
ISSN: 0193-4120 Page No. 2659 - 2673

Table 2 — The Main Parameters of the First LHT

Sample	Power (W)	Speed (mm/s)	Defocusing Distance (mm)	Scan Times (times)
F-0	180	2	+30	0
F-1	180	2	+30	3
F-2	180	2	+30	5

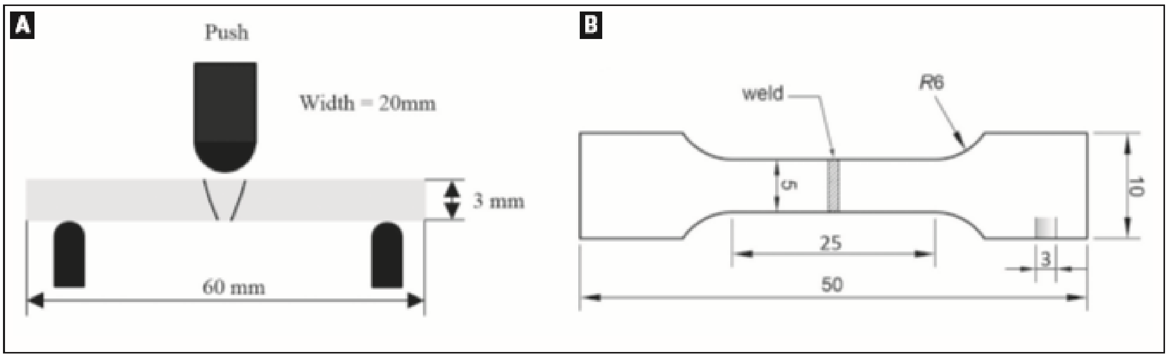

Fig. 3 — Sizes of test samples: A — Experimental device and sizes of bending samples; B — sizes of tensile samples.

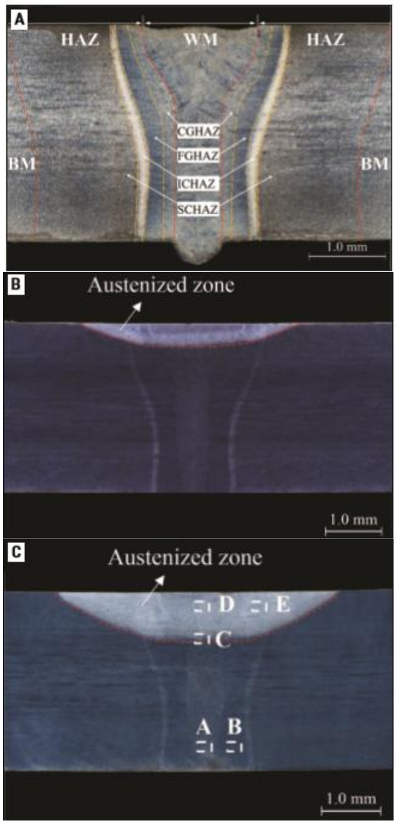

Fig. 4 — Optical microscopy micrographs of joints under different parameters: A — F-0 joints; B — F-1 joints; C — F-2 joints.

III. Experimental Results

Microstructures and Hardness after the First Laser Heat Treatment:

Microstructures of joints:

The OM micrographs of joints under various first LHT parameters are given in Fig. 4. The microstructures of laser-welded joints without LHT (F-0 joints) were introduced in a past work (Ref. 23). As Fig. 4A appears, the F-0 joints were made out of the WM and HAZ. The HAZ can be separated into coarse-grained HAZ (CGHAZ), fine-grained HAZ (FGHAZ), intercritical HAZ (ICHAZ), and subcritical HAZ (SCHAZ).

The microstructures in WM, CGHAZ, and FGHAZ are primarily strip martensite. The ICHAZ is made out of ferrite and martensite, and the microstructures in the SCHAZ are tempered martensite with ultrafine accelerated carbides. As represented in Fig. 4B and C, the microstructures of joints were clearly influenced by the first LHT. After the first LHT, the joints could be generally partitioned into the austenized zone and the treating zone. As the laser filtered around the upper surface where the temperature was higher, the austenized zone near the face was probably shaped because of austenization. Moreover, the microstructures in the zone were fundamentally unique with different zones. Since the laser spot was rectangular, the bowlshapedaustenized zone (on cross area) with incline sides and level base was framed. It was discovered that the more prominent austenized zone showed up in F-2 joints with ale heat input. As indicated by the Fe-C stage graph, the part austenization happens when the temperature is more than Ac1. So it tends to be guessed that the zones other than the austenized zone were treated with under Ac1 temperature. In particular, the zones outside of the austenized zone were in the hardening scope of temperature during the first LHT.

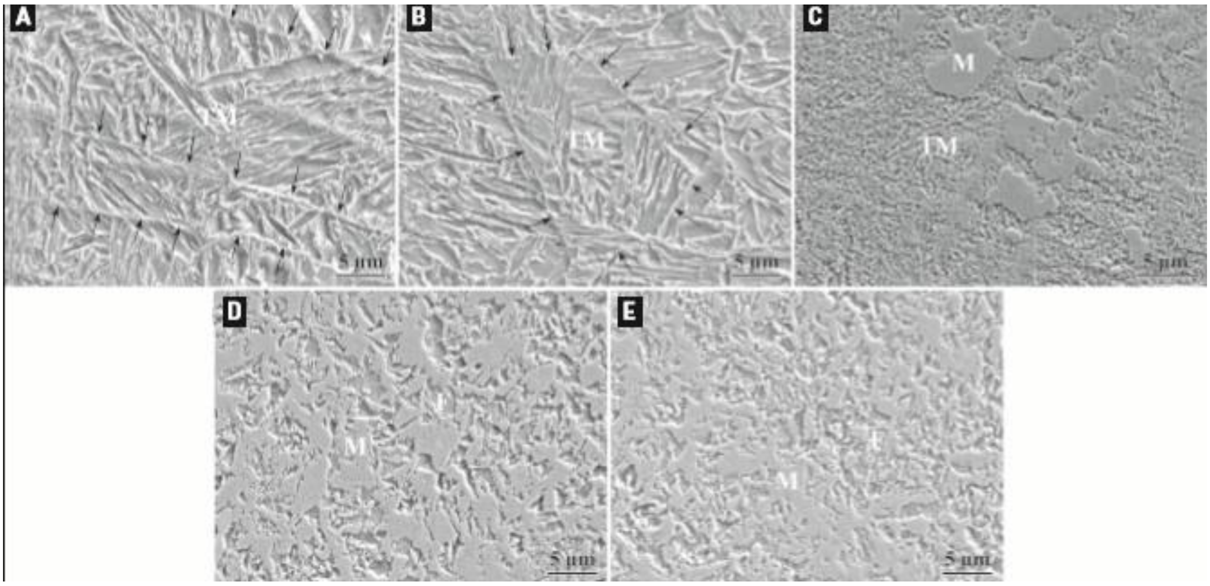

Fig. 5 — Scanning electron microscopy micrographs in different zones marked in Fig. 4C: A — WM at back; B — CGHAZ at back; C — around boundary of the austenite zone; D — WM in the austenite zone; E — HAZ in the austenite zone.

The SEM micrographs in various zones set apart in Fig. 4C are given in Fig. 5. In the hardening zone, the first microstructures of the WM and HAZ before LHT were slat martensite. As appeared in Fig. 5A and B, after the first LHT, the slat structure was as yet neat with a reasonable austenite limit (set apart by dark bolts) in the WM and HAZ. The high-amplification SEM micrographs of various zones are appeared in Fig. 6. Relating micrographs of the WM and HAZ in the treating zone are given in Fig. 6A and B, separately. There was practically no distinction between the microstructural highlights of the WM and HAZ in the treating zone. A lot of encourages were found on the network of tempered martensite. A large portion of the encourages resembled short poles with sizes of 0.1 ~ 0.2 μm. Evident accelerate conglomeration was found.

To recognize the creation of the encourages, cold field discharge high-goals SEM (Model: HITACHI SU8220) was utilized. The surface dispersions of various components are shown in Fig. 7. As Fig. 7A appears, loads of accelerates can be obviously observed. It was discovered that the surface circulations of C (found in Fig. 7B) and Fe (found in Fig. 7C) components were lopsided while the Cr (found in Fig. 7D), Mn (found in Fig. 7D), Si (found in Fig. 7F), and Ni (found in Fig. 7G) components were very much appropriated, which demonstrates that the structure of hastens has something to do with C and Fe rather than Cr, Mn, Si, and Ni. The stacking aftereffect of microstructures and dispersion of the C component (found in Fig. 7H) shows that the appropriations of encourages and C were in acceptable understanding. Figure 7I shows

May – June 2020
ISSN: 0193-4120 Page No. 2659 - 2673

the component circulations of C and Fe. It was discovered that the accelerates were somewhat wealthy in C and had less Fe comparative with the encompassing lattice.

Table 3 — The Main Parameters of the Second LHT

Sample	Power (W)	Speed (mm/s)	Defocusing distance (mm)	Scan times (times)
S-1	120	2	+50	4
S-2	120	2	+50	6

Table 4 — Mechanical Property Test Results of BM and Joints after the First LHT

Sample	Scan Times (times)	Back-Bending Angle (deg)	Face-Bending Angle (deg)	Tensile Strength (MPa)	Elongation (%)
BM	—	180	180	1653	9.0
F-0	0	30	28.5	1519	5.3
F-1	3	50	37	1412	6.2
F-2	5	> 90	62	1280	8.5

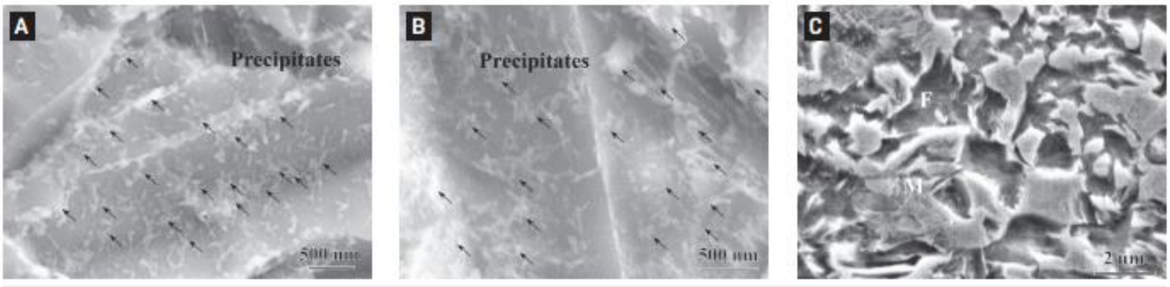

Fig. 6 — High-magnification SEM micrographs: A — WM in the tempering zone; B — CGHAZ in the tempering zone; C — WM in the austenite zone.

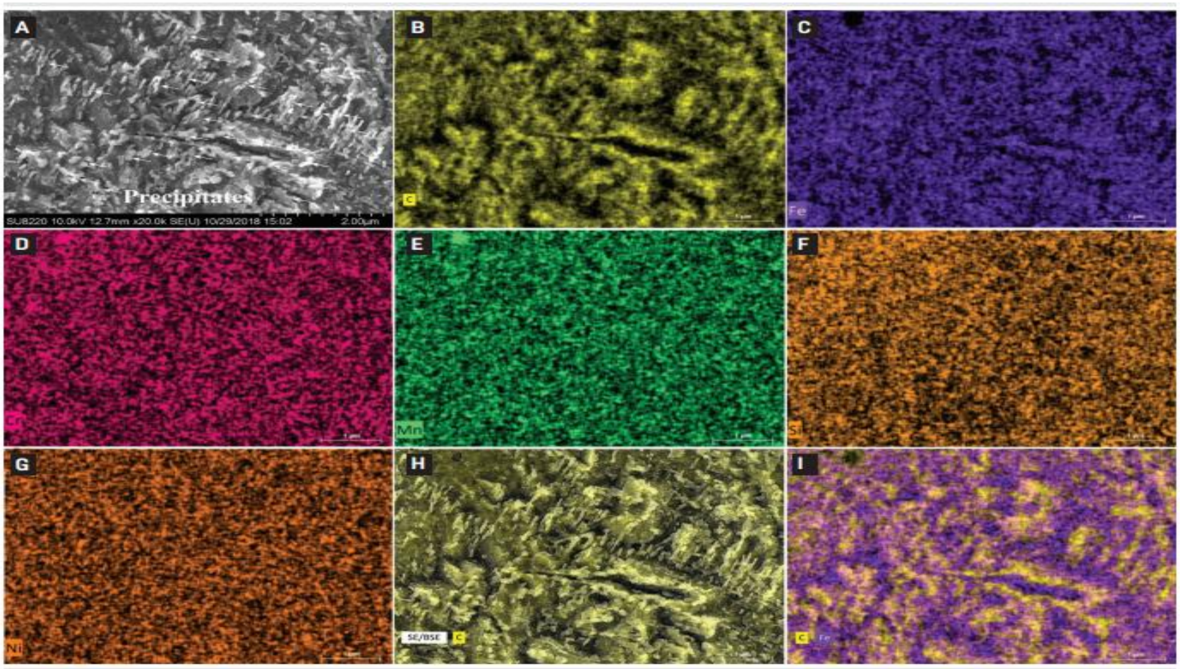

Fig. 7 — Surface distribution of different elements: A — Joint microstructures; B — distribution of C; C — distribution of Fe; D — distribution of Cr; E — distribution of Mn; F — distribution of Si; G — distribution of Ni; H — stacking distribution of microstructures and C; I — stacking distribution of C and Fe.

The austenized zone had a generously unique microstructure contrasted with the treating zone. It was found that the first martensite was changed into the dualphase structure, which may result from fractional austenization during the first LHT. As showed in Fig. 4B and C, it was hard to recognize the welds and HAZ in the austenized zone, which suggests that the microstructures of the entire zone were comparative. As investigated already, the austenized zone was shaped when the temperature was more than Ac1. Figure 5C shows the microstructures at the limit of the austenized zone. It was discovered that the huge structure showed up on the tempered martensite lattice. As showed in Fig. 5D and E, the microstructures of the unique WM and HAZ were comparable, which comprised of two particular stages. It was hypothesized that the enormous structure in the double stage microstructures was martensite islands, what's more, the other stage with polygonal morphology was ferrite. The high-amplification SEM micrographs of the WM in the zone are appeared in Fig. 6C, which were for the most part made out of double stage structures, and no undeniable carbides were found. Probably, the greater part of the first hastened carbides had broken up in the austenite and supersaturated in the martensite. The presence of the austenized zone infers the heterogeneity of the mechanical property .

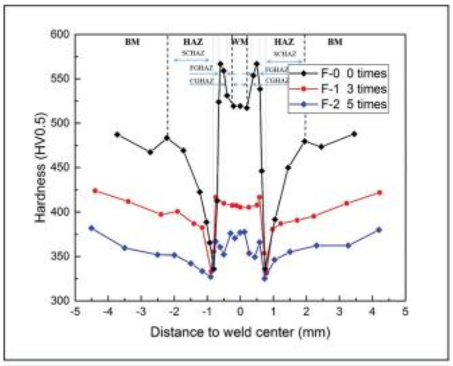

Fig. 8 — Microhardness distribution at the back of joints under the first LHT parameters.

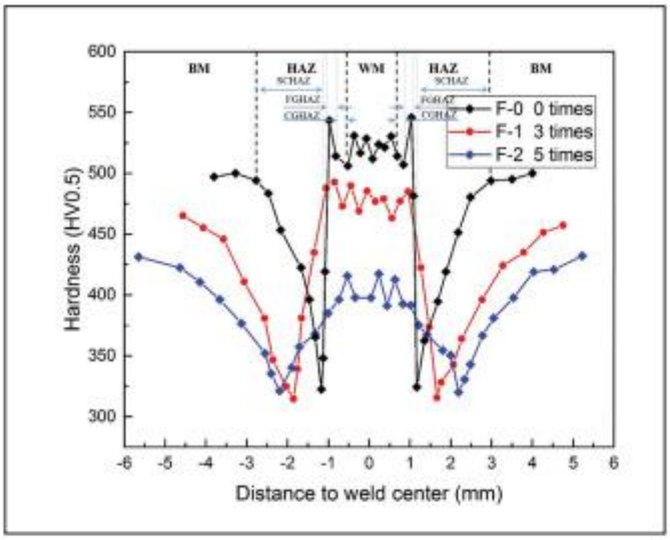

Fig. 9 — Microhardness distribution at face of joints under the first LHT parameters.

Table 5 — Mechanical Property Test Results of Joints After the Second LHT

Sample	Scan Times (times)	Face-Bending Angle (deg)	Tensile Strength (MPa)	Elongation (%)
S-1	4	78	1245	8.7
S-2	6	>90	1205	9.1

IV. Microhardness of joints.

The microhardness appropriations at the rear of joints under various parameters are given in Fig. 8. As outlined in Fig. 8, the hardness of joints without LHT (F-0 joints) differed fundamentally. Comparable circulations were distributed in a past report (Ref. 23). The hardness of WM, CGHAZ, and FGHAZ was more than 520 HV, higher than that of the base metal. A sharp decrease happened in the ICHAZ as ferrite showed up, which concurs with related reports (Ref. 5). The hardness in the zone diminished from 520 HV to around 400 HV. The base hardness was acquired in the SCHAZ, near the ICHAZ. The incentive in the zone was around 340 HV. The hardness step by step expanded from the SCHAZ to the base metal as the top temperature of the welding warm cycle diminished. It can be discovered that the most extreme hardness distinction of the entire joints was around 240 HV, and particular hardness valley existed in the delicate zone, which probably prompts poor bowing property because of strain fixation. As Fig. 8 shows, the

May – June 2020
ISSN: 0193-4120 Page No. 2659 - 2673

hardness circulations at the rear of joints after the first LHT would in general be increasingly uniform, which suggests that the first LHT was useful in wiping out the joint's inhomogeneity. It was discovered that the hardness at the weld and the HAZ diminished in general while the base hardness at the SCHAZ stayed about the equivalent. This can be attributed to the warming temperature at the rear of joints during LHT, which might be in the scope of treating temperature yet at the same time under Ac1. At the point when the joints were treated multiple times (F-1 joints), the hardness around the weld metal was around 420 HV, far beneath the first 520 HV. Moreover, the hardness estimations of SCHAZ additionally dropped altogether with the exception of the base worth. The greatest hardness distinction of the joints was around 100 HV. When the sweep times were expanded to multiple times (F-2 joints), the hardness of the entire joints diminished further and conveyed all the more consistently. The hardness distinction was dropped to pretty much 50 HV.

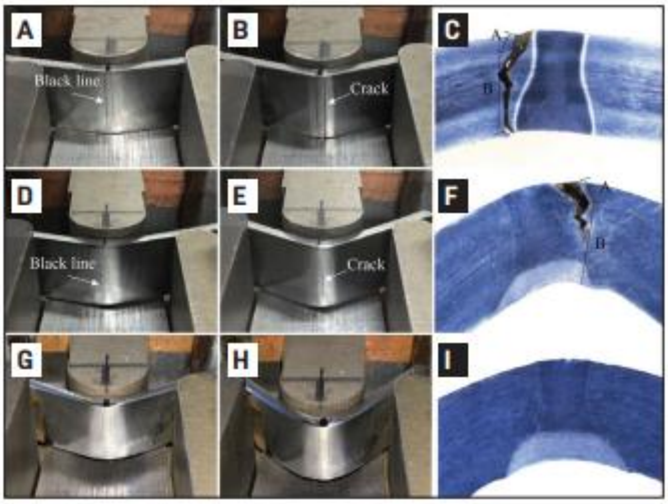

Fig. 10 — Back-bending process and fracture sections of joints under the first LHT parameters: A–C — F-0 joints; D–F — F-1 joints; G–I — F-2 joints.

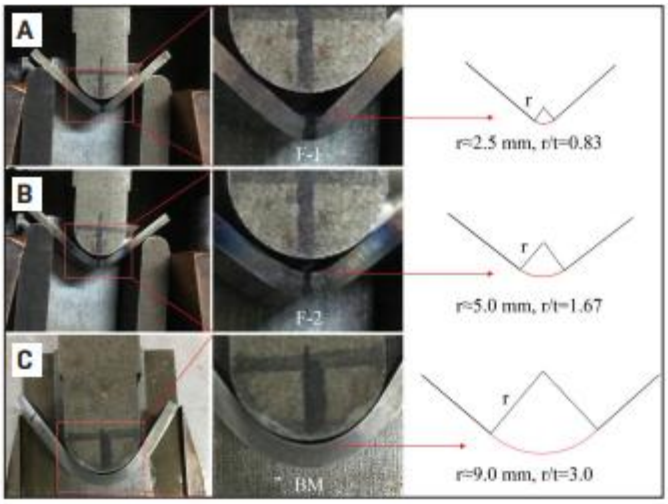

Fig. 11 — Joint appearances after the bending test: A — F-1 joints; B — F-2 joints; C — base metal.

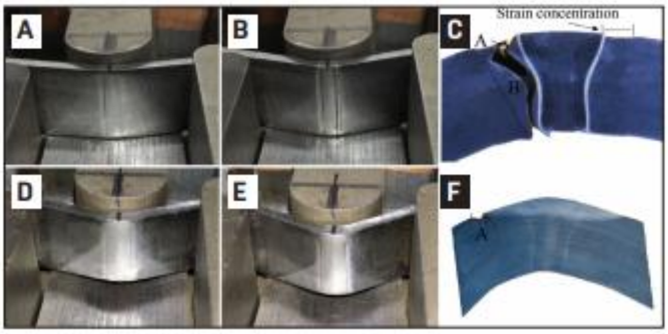

Fig. 12 — The face-bending process and fracture sections of joints under the first LHT parameters. A–C — F-0 joints; D–F — F-2 joints.

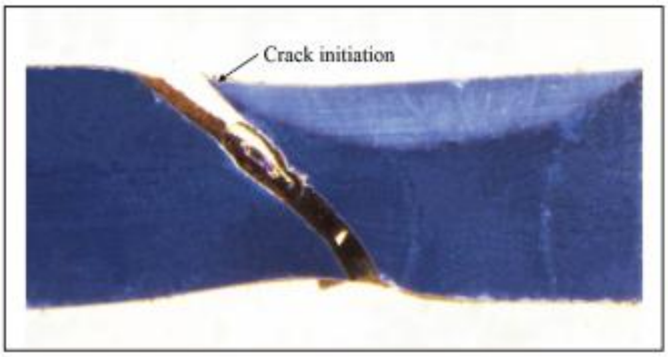

Fig. 13 — Fracture sections of F-2 joints after tensile testing

The microhardness disseminations at the essences of joints under various parameters are given in Fig. 9. Enormous dissipates were seen, demonstrating inhomogeneity of joints. As Fig. 9 demonstrates, for the joints without LHT (F-0 joints), the microhardness conveyance at the appearances was

TEST Engineering & Management
May – June 2020
ISSN: 0193-4120 Page No. 2659 - 2673

comparative with that at the rear of joints. The hardness valley was self-evident. There were as yet gigantic contrasts of hardness significantly after the first LHT. For F-1 joints, the hardness around the focal point of the austenized zone was around 480 HV. The hardness esteem diminished slowly from the center to the sides. The least hardness existed around the sides of the
austenized zone, and the worth was 340 HV, comparable with F-0 joints. The hardness valley existed around the sides of the austenized zone, which may restrict the face-twisting property of joints. For F-2 joints, the hardness circulations were like F-1 joints aside from the incentive around the center of the austenized zone. The hardness distinction of the joints was still around 100 HV. At the point when the sweep times expanded from three to multiple times, the austenized zone extended and the hardness esteem around the center decreased, which may be because of the way that high warmth input brings about a bigger influenced zone and a shorter cooling rate.

V. Mechanical Properties After The First Laser Heat Treatment

The back-bowing, face-twisting, and malleable trial of the assupplied condition of the base metal and joints under Table 2 parameters were completed. The outcomes are appeared in Table 4.

Back-bowing test outcomes. The outcomes show the most extreme back-twisting edge was changed under various parameters. For the joints without LHT (F-0 joints), the twisting deformability was lacking with just around a 30- deg twisting edge. After the LHT, the back-bowing edge of joints improved altogether. For the joints filtered three times by laser (F-1 joints), the point expanded to around 50 deg. With the further increment of sweep times to multiple times (F2 joints), the more than 90-deg back-bowing edge was gotten, which met the application prerequisites (Ref. 16). It shows that the first LHT is a successful method to improve the back-bowing property of joints.

The back-bowing advancement and crack segments of the joints under various parameters are given in Fig. 10. As Fig. 10A and B appear, for the joints without LHT (F-0 joints), dark lines steadily showed up on the two sides of the weld, and at that point the joints split along one of them, which may be because of the nearness of strain focus. Figure 10C shows the F-0 joints cracked around the "dark line." In the twisting test, the significant plastic distortion happened at the surface where the material encountered the greatest distracting tractable pressure. In this manner, the crack may happen specially at the highest point of around the ICHAZ (found in Fig. 10C) and afterward spread around the zone since the relating hardness was the most reduced. The crack way can be isolated into two sections: quick extension zone and moderate development zone. After it started at the top surface of around the ICHAZ, the break extended quickly along a line (way A) to discharge the vitality gathered in the beginning time. At that point the break extended gradually (way B) with the further development of the bowing punch. The way was slanted to the ICHAZ since the hardness diminished step by step near the ICHAZ.

At long last, the examples cracked totally in the SCHAZ. The bowing advancement and crack areas of F-1 joints are appeared in Fig. 10D–F. It was discovered that a comparative marvels occurred, yet the dark lines were not all that conspicuous with the same edge. A more extensive twisting point was acquired, and the joints at last bombed similarly situated. The break way was additionally like the F-0 joints since the changing law of hardness is the equivalent. The split additionally started around the top surface and extended along ways An and B. As Fig. 10G and H appear, no conspicuous strain focus showed up on the F2 joints, and a more than 90-deg twisting edge was acquired effectively without evident splits on the joint's surface (found in Fig. 10H and I). The relative twisting sweep is the proportion of the inward range r of the bowing example to the plate thickness t. The joint and base metal appearances after the bowing test are given in

May – June 2020
ISSN: 0193-4120 Page No. 2659 - 2673

Fig. 11. It was discovered that there exists evident contrasts in the relative bowing span under various LHT parameters. As Fig. 11A shows, the bowing span of F-1 joints was essentially littler than the twisting punch range to leave a great deal of space among tests and the punch. Estimated dependent on the geometric strategy, the normal inward sweep of F-1 joints was about 2.5 mm, and the relative bowing span was just about 0.83. As Fig. 11B shows, for F-2 joints, the fit circumstance of F-2 joints between the examples and bowing punch improved to some degree. The internal span was about 5.0 mm and the relative bowing range was about 1.67. As Fig. 11C shows, the base metal bowing examples remained nearby to the bowing punch, and a solid match was accomplished. The twisting sweep was about 9.0 mm, essentially equivalent to the sweep of the punch. The relative twisting span was 3.0.

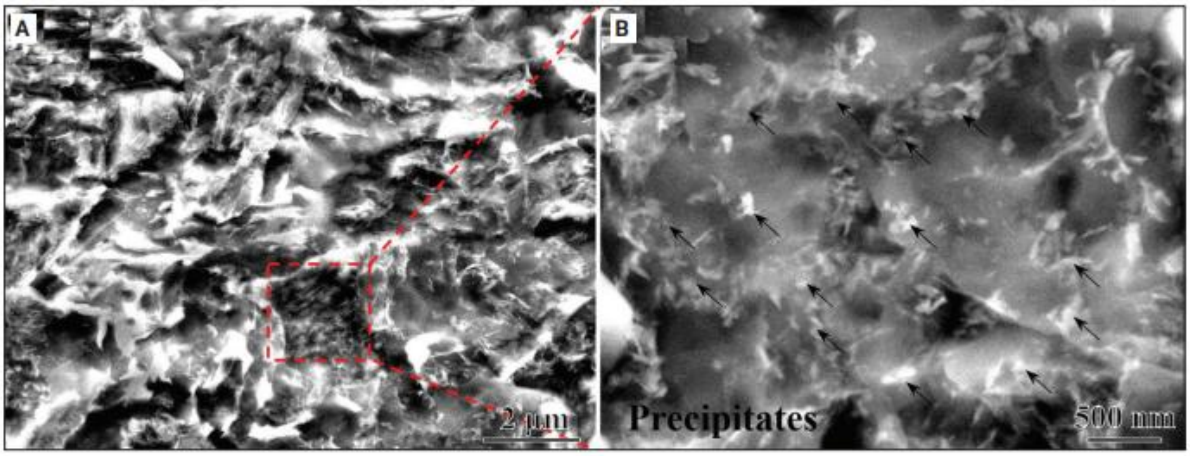

Fig. 14 — SEM micrographs of the austenite zone after the second LHT (S-2 joints): A — 0-k magnification; B — 30-k magnification.

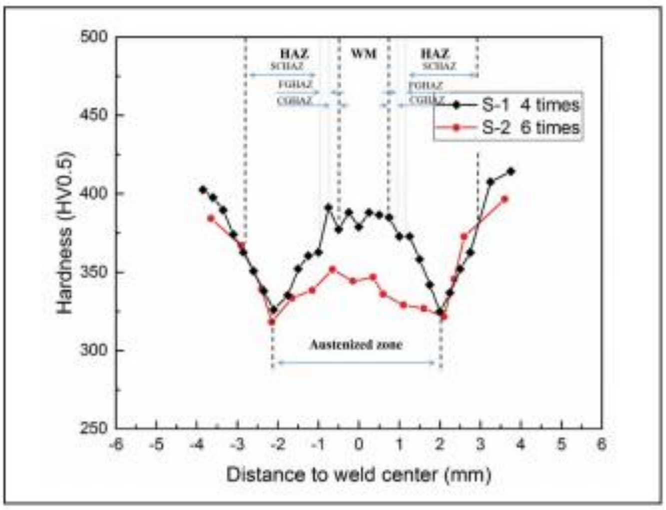

Fig. 15 — Microhardness distribution at the face of joints under the second LHT parameters.

Face-twisting Test Outcomes.

The face-bowing aftereffects of joints under various parameters are appeared in Table 4. It ought to be noticed that the face-bowing points were as yet unacceptable after the first LHT. For the joints without LHT, the point was just about 28.5 deg, comparative with the back-twisting point. After LHT, the point was improved. With three sweep times, the face-twisting point of joints (F-1 joints) expanded marginally to 37 deg. With the further increment of sweep times to multiple times (F-2 joints), the face-bowing point expanded to 62 deg. The improvement of face-bowing point was in acceptable concurrence with hardness circulations at the essence of joints (found in Fig. 9), which will in general be progressively uniform after the first LHT. Nonetheless, as appeared in Fig. 9, the hardness valley despite everything exists much after five output times, which can't be dispensed with by the enhancing of the first LHT. This would restrain the facebending property of joints. In particular, the face-twisting property was not good after the first LHT. The twisting procedure and crack areas of the joints under various parameters are appeared in Fig.

May – June 2020
ISSN: 0193-4120 Page No. 2659 - 2673

12. As showed in Fig. 12A–C, much the same as the back bowing, the dark lines additionally showed up because of strain focus. The plastic misshapening zone can be plainly found in the figures while the weld metal disfigured a bit. The crack areas (found in Fig. 12C) demonstrate that the strain fixation zone was situated in the SCHAZ where the hardness was less contrasted with different zones. The dark lines were near the ICHAZ. The crack procedure was additionally made out of the quick development (stage An) and slow extension (stage B). For F-1 joints, plastic twisting additionally focused, and the split started at the limit of the austenized zone rather than around the first ICHAZ (found in Fig. 12D–F) as the base hardness showed up in the sides of the austenized zone, which is steady with hardness appropriation.

A comparative marvel occurred during the face bowing of F-1 joints. Specifically, the first LHT would constrain the face-bowing property of joints, and the second LHT was expected to take care of the issue.

Ductile Test Outcomes

The ductile test consequences of joints after the first LHT are given in Table 4, which uncover a significant impact of LHT on mechanical properties. For base metal examples with the sizes appeared in Fig. 3B, the ductile quality was roughly 1653 MPa with the extension of 9.0%. In the untreated express, the F-0 joints had ductile quality of roughly 1519 MPa and indicated a joint proficiency of over 93.0%. As Table 4 shows, the ductile quality of joints diminished step by step with the expansion of examine times, which implies the first LHT debilitated the laserwelded joints. For F-1 joints, the rigidity was about 1412 MPa. With the further increment of sweep times to five times, the elasticity decreased to 1280 MPa. This may result from the expansion of warmth input, yet the quality still remained far over 1000 MPa of circular segment welded joints. To be specific, the LHT could limit quality loss of joints. In the untreated express, the F-0 joints demonstrated a low homogeneous plastic distortion with an absolute extension of about 5.3%. In correlation, the joints after LHT indicated a bigger scope of homogeneous plastic twisting. The F-1 joints had an extension of about 6.2%, and the F-2 joints demonstrated an extension of 8.5%. It very well may be presumed that the LHT was useful to the formability of joints. The outcomes concurred well with discoveries of correlational research (Ref. 30). The break areas of F-2 joints after pliable testing are given in Fig. 13. It very well may be discovered that the break way was a 45-deg incline, which is near the austenized zone. In this way, it was speculated that the break may start at the edge of austenite since the hardness around the zone is the most minimal. The split at that point reached out along the 45-deg shear plane lastly severed. Specifically, the presence of a mellowed zone in the circumferential austenized zone debilitated and constrained the quality of joints.

VI. Microstructures and Hardness after the Second Laser Heat Treatment

After the first LHT, the second LHT was utilized to improve the face-bowing property of joints. To get good face-and back-twisting points, all the second LHT were received dependent on F-2 joints. Lower power was utilized in the second LHT to relax the austenized zone rather than the hardening zone. Since the treating zone was practically unaffected, perception and hardness testing for the microstructures were just performed on the austenized zone.

Microstructures of joints. The SEM micrographs of joints after the second LHT (S-2 joints) are given in Fig. 14. As Fig. 14A shows, the zone kept the first double stage microstructures with noticeable accelerates. Through the highmagnification micrographs in Fig. 14B, the accelerates were like short bars with sizes of 0.1 ~ 0.2 □ m, much the same as the precipitation carbides in the hardening zone after the first LHT. It was estimated that comparable microstructure change happened in the austenized zone after the second LHT.

May – June 2020
ISSN: 0193-4120 Page No. 2659 - 2673

VII. Microhardness of Joints

The microhardness appropriations of joints after the second LHT are outlined in Fig. 15. The scopes of the austenized zone and unique subzones of the weld were set apart in the figure. It tends to be seen that, after the second LHT, the hardness in the austenized zone diminished while the qualities outside fundamentally kept invariant. For S-1 joints, the hardness around the focal point of the austenized zone diminished to around 385 HV. As the first least hardness stayed unaltered, the hardness distinction decreased to 60 HV and the hardness valley despite everything existed, which may restrain the deformability of joints. With the expansion of check times to multiple times (S-2 joints), the hardness in the austenized zone diminished to 345 HV, and the diverse worth decreased to 20 HV. This implies the precarious hardness angle underneath the face was totally smoothed out to a comparable hardness.

VIII. Mechanical Property after the Second Laser Heat Treatment

As the second LHT was performed dependent on F-2 joints with less force, it was estimated that the back-bowing edge was wide enough after the second LHT. Along these lines, as it were the face-twisting and pliable trial of joints under Table 3 parameters were done. The outcomes are given in Table 5. Face-twisting test outcomes. For the joints examined four times constantly LHT (S-1 joints), the face-bowing edge of joints was improved 62–78 deg. With the sweep times expanding to multiple times (S-2 joints), the bowing deformability was additionally improved, and a more than 90-deg face-bowing point was gotten. To be specific, the second LHT could successfully improve the face-bowing property of the joints. The face-bowing procedure and crack areas under various parameters are appeared in Fig. 16. A represented in Fig. 16A and B, for S-1 joints, the strain focus around the side of the austenized zone despite everything existed lastly brought about breaking, which was like the procedure of F-2 joints. Nonetheless, the comparing point was essentially more extensive. As appeared in Fig. 16C, contrasted with F-2 joints, the weld metal and austenized zone of S-1 joints had been significantly twisted before the split. Apparently, the mollified austenized zone took an interest in the bowing misshapening be that as it may, at last despite everything bombed around the sides of the austenized zone with a comparable break way. For S-2 joints, a more than 90-deg point was gotten without splitting (found in Fig. 16D and E), and no conspicuous plastic disfigurement fixation was watched. As found in Fig. 16F, the austenized zone disfigured altogether with the expansion the circumferential way and diminishing the outspread way. The appearances of S-1 and S-2 joints after the bowing test are given in Fig. 17. Contrasted and S-2 joints, there was more space among tests and the punch, which inferred a littler internal span during the twisting test. As Fig. 17A shows, the normal inward range of S-1 joints was simply about 2.3 mm, and the relative twisting range was about 0.77. For the S-2 joints (found in Fig. 17B), the inward range was about 3.4 mm, and the relative twisting range was about 1.13.

Elastic test outcomes. The ductile test results after the second LHT can likewise be found in Table 5. As outlined in the table, little quality misfortune happened after the second LHT. For the joints with four output times (S-1 joints), the pliable quality decreased to 1245 MPa. With the expansion of output times to multiple times (S-2 joints), the quality diminished to 1205 MPa with about 73% joining productivity. In the mean time, the stretching was improved from 8.7 to 9.1%. To be specific, the second LHT further undermined the rigidity of joints. In any case, the decrease was less as the shortcoming zone of joints had just shaped after the first LHT. The quality of joints after the second LHT was still fundamentally higher than the 1000 MPa of the bend welded joints.

May – June 2020
ISSN: 0193-4120 Page No. 2659 - 2673

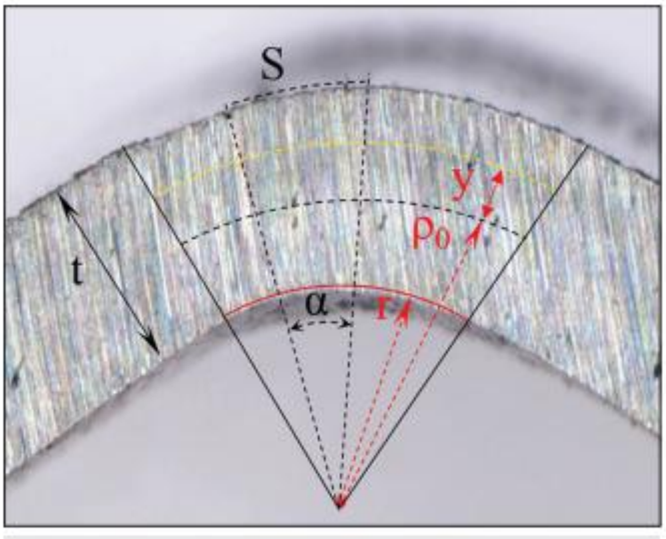

Fig. 18 — Geometrical relationship of bending samples.

IX. Conclusion

Homogenization of Microstructure and Hardness Distribution of Joints

Homogenization of the microstructure occurred in various zones of joints after the LHT. In light of the consequences of microstructures of joints after the first LHT, it was gathered that the hardening change of martensite happened in the hardening zone. The component conveyances in Fig. 7 demonstrates that the organization of the accelerates is identified with C and Fe. In view of important references (Refs. 39, 40), the change temperature of □-carbide to cementite is about 260° ~ 310°C in low-composite steel. The accelerated stage in the martensite is essentially □-carbide when the treating temperature is under 260°C. At the point when the treating temperature comes to 260° ~ 310°C, the encouraged □-carbide in the martensite changes to cementite. In this way, it is estimated that the accelerates are cementite, which is made out of rich C (6.67- wt-%, hypothetical substance in cementite) and poor Fe (93.33 wt-%, hypothetical substance in cementite) contrasted with the normal component substance of the base metal. This deduction compares well to the aftereffects of revealed works (Refs. 40, 41). The precipitation of cementite is an average attribute of martensite treating. In the hardening procedure, the carbon supersaturated in martensite accelerates as carbides, and at that point the first martensite was disintegrated into ferrite and carbides (Ref. 41). The carbides collected and developed with the high-hardening temperature (Refs. 42, 43). In the austenized zone, monstrous microstructures showed up after the first LHT. In view of investigation of the arrangement system (Ref. 44) and morphology (Refs. 41, 45), the structures were decided to be martensite islands, which for the most part contain a lathy substructure (Refs. 41, 46). It is assumed that halfway austenization happened during LHT, and the encouraged carbides began to break down into the austenite. Subsequent to cooling, the austenite changed into martensite and the ferrite was held. Near the face, the pinnacle temperature rose step by step, which prompted the expansion of new martensite. Subsequently, the double stage microstructures in the austenized zone were martensite islands and polygonal ferrite. Probably, the vast majority of the first encouraged carbides of joints had disintegrated in the austenite and supersaturated in martensite. In this way, after the second LHT, the carbide encouraged again from the martensite.

As Fig. 14 shows, for the joints after the second LHT, the encourages in the austenized zone were comparative with the precipitation in treating zone. It is conjectured the encourages in the austenized zone were likewise cementite. To be specific, the double stage microstructures in the austenized zone were tempered after the second LHT. In this way, the LHT relieved the microstructural contrast of joints since the microstructures in various zones changed over to the tempered structure after two phases of laser heat treatment.

The homogenization of the microstructure unavoidably had an impact on the hardness dispersion of joints. As indicated by a past examination (Ref. 23), the base hardness of joints came about because of high-temperature treating of the SCHAZ. A comparative marvel happened around the side of the austenized zone after the first LHT. As appeared in Figs. 8, 9, and 15, the base hardness at the face and back of joints changed minimal after the LHT. Since the LHT prompted the general hardening advancement in various zones of joints, the hardness dissemination definitely diminished. As appeared in Fig. 8, the hardness distinction at the rear of joints diminished from 240 to 50 HV after the first LHT. The hardness valley was not all that obvious. A comparable wonders additionally happened in the austenized zone. As appeared in Figs. 9 and 15, the hardness contrast at the essences of joints decreased from 100 to 20 HV after the second LHT. In particular, the hardness uniformly circulated after the two phases of laser heat treatment, which suggests a mechanical homogeneity. It very well may be presumed that the LHT is useful for uniform mechanical properties at the back and face of joints.

References

1. Xie, Z. J., Shang, C. J., Wang, X. L., et al. 2018. Microstructure-property relationship in a low carbon Nb-B bearing ultra-high strength steel by direct-quenching and tempering. Materials Science and Engineering A 727(6): 200–207. DOI: 10.1016/j.msea.2018.04. 086
2. Wen, C., Wang, Z., Deng, X., et al. 2018. Effect of heat input on the microstructure and mechanical properties of low alloy ultrahigh strength structural steel welded joint. Steel Research International 89(6): 1700500-1 to 1700500-9. DOI: 10.1002/srin. 201700500
3. Erdem, M., Mehmet, A., and Karabulut, M. 2016. Investigation of mechanical, microstructural, and machining properties of AISI 420 martensitic stainless steel welded by laser welding. International Journal of Advanced Manufacturing Technology 85(1–4): 481–492. DOI: 10.1007/s00170-015-7924-2
4. El-Batahgy, A. M., Miura, T., Ueji, R., and Fujii, H. 2016. Investigation into feasibility of FSW process for welding 1600 MPa quenched and tempered steel. Materials Science and Engineering A 651: 904–913. DOI: 10.1016/j.msea.2015.11.054
5. Janicki, D. 2014. Disk laser welding of armor steel. Archives of Metallurgy and Materials 59(4): 1641–1646. DOI: 10.2478/ amm-2014-0279
6. Pek, N. E., and Elaldi, F. 2012. Analysis of welding groove angle and geometry on strength of armor steel. Materials and Manufacturing Processes 27(12): 1437–1441. DOI: 10.1080/10426914. 2012. 709343
7. Hanhold, B., Babu, S. S., Cola, G. M., and Ream, S. 2012. Investigation of HAZ softening in laser welding of AHS/high hardness steels. 9th International Conference on Trends in Welding Research, American Society for Metals, pp. 19–25. Chicago, Ill. ASM International.
8. Murthy, N. K., Ram, G., and Murty, B. S. 2014. Carbide-free bainitic weld metal: A new concept in welding of armor steels. Metallurgical & Materials Transactions B 45(6): 2327–2337. DOI: 10.1007/s11663-014-0120-1
9. Magudeeswaran, G., Balasubramanian, V., and Balasubramanian, T. S. 2013. Effect of welding consumables on tensile and impact properties of shielded metal arc welded high strength, quenched and tempered steel joints. Science & Technology of Welding & Joining 13(2): 97–105. DOI: 10.1179/174329307X249432
10. Oyyaravelu, R., Kuppan, P., and Arivazhagan, N. 2016. Metallurgical and mechanical properties of laser welded high strength low alloy steel. Journal of Advanced Research 7(3): 463–472. DOI: 10.1016/j.jare.2016.03.005
11. Liu, T., Yang, L. J., Wei, H. L., and Qiu, W. C. 2017. Composition change of stainless steels during keyhole mode laser welding. Welding Journal 96(7): 258-s to 270-s.
12. Gu, Z., Yu, S., and Han, L. 2012. Influence of welding speed on microstructures and

properties of ultra-high strength steel sheets in laser welding. ISIJ International 52(3): 483–487. DOI: 10.2355/isijinternational.52.483

13. Fahlstrom, K., Persson, K. A., and Larsson, J. K. 2016. Evaluation of laser weldability of 1800 and 1900 MPa boron steels. Journal of Laser Applications 28(2): 022426-1 to 022426-7. DOI: 10.2351/1.4944102
14. 14.Manikyam Sandeep,“ Experimental Investigation and Optimization of MRR, Surface Roughness and Overcut of AISI 316 Stainless Steel in EDM using Taguchi Method ” in International Journal of Advanced Science and Technology ISSN: 2005-4238 IJAST VOLUME 28 ISSUE 16 DEC2019
15. Manikyam Sandeep,“ Experimental Investigation and Optimization of MRR, Surface Roughness and Overcut of AISI 316 Stainless Steel in EDM using Taguchi Method ” in International Journal of Advanced Science and Technology
16. ManikyamSandeep,“Enhancement and Gray Relational Analysis ofEn 31steel Using Parameters Of Wire Cut Electric Discharge Machine” inICMMSE,MaterialsToday:proceedings,Elsevier**ISSN:** 2214-7853
17. ManikyamSandeep, “A mobile robotic welding robot will be verified both theoretically and empirically using AWS and ASTM standards” in International Journal Of Recent Technology And Engineering ISSN: 2277-3878 VOLUME 8 ISSUE -5.
18. Manikyam Sandeep “Optimization of analytical modelling of aluminum-multiwall carbon nanotube composites**”** Materials Today: proceedings, Elsevier **ISSN:** 2214-7853 https://doi.org/10.1016/j.matpr.2019.08.141